Nat. Hazards Earth Syst. Sci., 10, 73–87, 2010
www.nat-hazards-earth-syst-sci.net/10/73/2010/

Natural Hazards and Earth System Sciences

Deformation pattern of the 6 and 7 April 2009, M_W=6.3 and M_W=5.6 earthquakes in L'Aquila (Central Italy) revealed by ground and space based observations

I. D. Papanikolaou[1,2], **M. Foumelis**[3], **I. Parcharidis**[4], **E. L. Lekkas**[5], **and I. G. Fountoulis**[5]

[1]Laboratory of Mineralogy & Geology, Department of Geological Sciences and Atmospheric Environment, Agricultural University of Athens, 75 Iera Odos Str., 118 55, Athens, Greece
[2]AON Benfield Hazard Research Centre, Department of Earth Sciences, Birkbeck College and University College London, WC1E 6BT, London UK
[3]Department of Geophysics – Geothermics, National and Kapodistrian University of Athens, Panepistimioupolis, Ilissia, 157 84, Athens, Greece
[4]Department of Geography, Harokopio University of Athens, El. Venizelou 70, Kallithea, 176 71, Athens, Greece
[5]Department of Dynamic, Tectonic and Applied Geology, National and Kapodistrian University of Athens, Panepistimioupolis, Ilissia, 157 84, Athens, Greece

Received: 15 September 2009 – Revised: 16 December 2009 – Accepted: 17 December 2009 – Published: 14 January 2010

Abstract. The deformation pattern of the 6 and 7 April 2009 M_W=6.3 and M_W=5.6 earthquakes in L'Aquila is revealed by DInSAR analysis and compared with earthquake environmental effects. The DInSAR predicted fault surface ruptures coincide with localities where surface ruptures have been observed in the field, confirming that the ruptures observed near Paganica village are indeed primary. These ruptures are almost one order of magnitude lower than the ruptures that have been produced by other major surrounding faults in the past. These faults have not been activated during the 2009 event, but have the capacity to generate significantly stronger events. DInSAR analysis shows that 66% (or 305 km^2) of the area deformed has been subsided whereas the remaining 34% (or 155 km^2) has been uplifted. A footwall uplift versus hangingwall subsidence ratio of about 1/3 is extracted from the mainshock. The maximum subsidence (25 cm) was recorded about 4.5 km away from the primary surface ruptures and about 9 km away from the epicentre. In the immediate hangingwall, subsidence did not exceeded 15 cm, showing that the maximum subsidence is not recorded near the ruptured fault trace, but closer to the hangingwall centre. The deformation pattern is asymmetrical expanding significantly towards the southeast. A part of this asymmetry can be attributed to the contribution of the 7 April event in the deformation field.

Correspondence to: I. D. Papanikolaou
(i.papanikolaou@ucl.ac.uk)

1 Introduction

On Monday 6 April 2009 a strong earthquake struck the city of L'Aquila and the surrounding villages producing extensive damages, about 300 fatalities and more than a thousand of injuries. The earthquake was assessed as a M_W=6.2 or M_L=5.8 (source INGV) or M_W=6.3 (USGS), having a normal faulting mechanism of N147° striking and dipping about 43° towards the SW and a focal depth at 9 km. InSAR, body wave seismology and GPS data determined a SW∼50° dipping normal fault with a maximum ∼0.6–0.9 m slip (Walters et al., 2009; Atzori et al., 2009; Anzidei et al., 2009). The epicenter was located a few km WSW from the city of L'Aquila which including the surrounding villages, hosts a population of about 100 000. This earthquake triggered two other events above Magnitude 5 both southeast and north of the mainshock, expanding the aftershocks distribution. In particular, about 40 h after the mainshock a M_W=5.6 or M_L=5.3 event occurred in Valle d'Aterno, about 4 km SW from the village of Fossa, whereas on 9 April a third event of M_W=5.4 or M_L=5.1 occurred near Campotosto about 16 km northwards L'Aquila (source INGV). Initially, the aftershock activity occurred near L'Aquila and towards the south-east of the town, whereas a couple of days later it migrated towards the NE at Barrete and Campotosto. The seismicity covers a rectangulary elongated area that is approximately 40 km long and 10–12 km wide trending towards the NW-SE (Chiarabba et al., 2009; Pondrelli et al., 2009).

Published by Copernicus Publications on behalf of the European Geosciences Union.

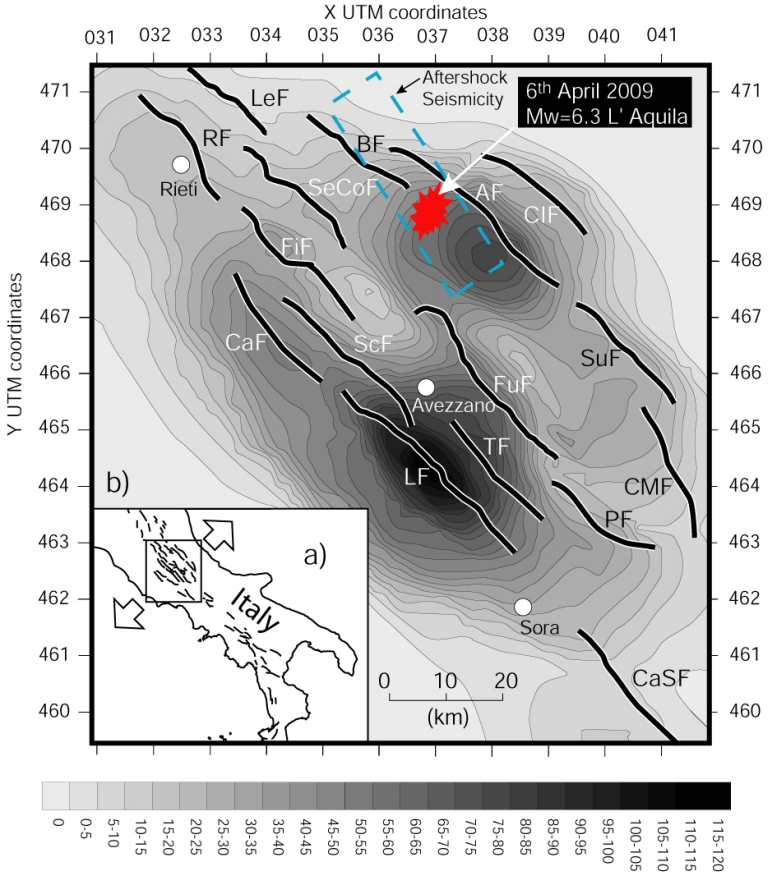

Fig. 1. (a) Map of the Italian Peninsula showing the active faults and the NE-SW extension occurring in Abruzzo (Modified from Roberts et al. 2002). **(b)** Map showing the epicentre of the 6 April 2009 earthquake and how many times each locality receives enough energy to shake at intensities ≥ IX over the last 18 000 yrs based on geological fault slip-rate data (modified from Roberts et al., 2004). The blue dashed rectangular represents the aftershock seismicity zone. The epicenter is located in an area that is characterized by a high frequency and lies in the hangingwall of three major faults (the L'Aquila, AF, the Barete, BF, and the Campo Imperatore, CIF, faults). The Barete (Arichia or Mt Marine) fault was activated in the seismic sequence of 1703 producing surface ruptures >10 km long, a maximum displacement of 1m and significant damage (IX intensity) to L'Aquila (Blumetti 1995). The Fucino Fault (FuF) was ruptured in 1915 (M=6.9–7.0), producing surface ruptures more than 20 km long devastating the entire Fucino Basin (X and XI intensity, 33 000 deaths, second most destructive earthquake in Italy).

2 Geological setting

The Apennines are part of the Alpine orogenic system that formed as a result of the subduction of Tethyan ocean crust and collision between African continental fragments and the Eurasian plate (Boccaletti et al., 1971; Doglioni et al., 1996). During the Upper Miocene-Lower Pliocene, extension and accretion of new oceanic crust occurred in the Tyrrhenian Sea west of Italy (Lucente et al., 1999). Active subduction of the Ionian sea beneath Calabria was occurring at the same time with a progressive eastward migration of compressional fronts (Malinverno and Ryan, 1986). By the late-middle Pliocene shortening ceased in the Tyrrhenian part of Central and Southern Italy (e.g. Patacca et al., 1990) and extension began in the Apennines (Cavinato and De Celles, 1999).

The earthquake occurred on one of the NW-SE trending normal faults that form part of the 800 km long segmented normal fault system (Fig. 1a) that accommodates the extension in the Apennines (e.g. Anderson and Jackson, 1987; Roberts et al., 2002). In the central Appenines faults are characterized by pure dip slip faulting with a mean fault slip direction of 222°±4° (Roberts and Michetti, 2004). These faults tend to generate strong events from $M = 5.5$ up to $M = 7.0$ and depending on the magnitude and the earthquake depth can produce from minor to severe damages and occasionally destruction (Michetti et al., 1996; Galadini and Galli, 2000; Roberts et al., 2004). It has to be noted that about 40 km southern from the 2009 L'Aquila earthquake in the Fucino basin, Italy experienced its second most destructive earthquake. Indeed, the

1915 Earthquake ($M_s = 6.9-7.0$) produced extensive surface ruptures >20 km long and devastated the entire Fucino basin (all villages situated within the basin suffered intensities X and XI in the MCS Mercalli-Cancani-Sieberg scale), causing 33 000 deaths (Oddone, 1915).

3 Historical record and seismic hazard of L'Aquila

Based on the historical record the town has suffered intensity IX or higher at least three times in the past (in 1349 AD, 1461 AD, and 1703 AD, INGV-DBM04 2004, Tertulliani et al., 2009). The 1703 ($M_W \sim 6.7$) event was part of a seismic sequence that struck the area. However, the damage of L'Aquila in 1703 is not attributed to the L'Aquila fault, but most probably to the nearby Barete fault that lies westwards (Fig. 1b). The Barete fault (or elsewhere known as the Arischia fault or Mt Marine fault) was activated during the final third earthquake of the sequence on 2 February 1703, where surface ruptures and liquefaction phenomena were reported near the village of Pizzoli (Blumetti, 1995).

Following the above, L'Aquila has been assessed as an area of relatively high seismic hazard using the typical Poissonian approach (Slejko et al., 1998; GNDT-SSN, 2001; Rebez et al., 2001). Romeo and Pugliese (2000) using a Poissonian approach estimated a high probability for a peak ground acceleration of 0.25 g in a 50 year period and estimated a very high time-dependent probability of 23.6% in the next 30 years of a $M_s > 6.3$ in L'Aquila. Boncio et al. (2004) assessed a maximum expected magnitude between 6.1 and 6.4 for the L'Aquilano fault that bounds the Aterno basin. Moreover, Pace et al. (2006) based on time dependent probabilities and a BPT distribution estimated for the year 2004 about 10% the probability for the next 50 years of rupturing of the Paganica segment that neighbours the town of L'Aquila and estimated a high probability of a peak acceleration exceeding 0.30 g in a 50 year period. Finally, seismic hazard maps based solely on geological fault slip-rate data (and thus independent from the historical record) also show that the hangingwall centre of the L'Aquila fault is characterised by high shaking frequency for intensities ≥IX (Fig. 1b) reaching up to 80 times over the last 18 000 yrs, implying that the area suffers a destructive earthquake approximately every 250±50 years (Roberts et al., 2004). This high frequency and short recurrence interval is attributed to the combined effects of three closely spaced major active faults (L'Aquila, Barete and Campo Imperatore faults) that can produce extensive damage in the town of L'Aquila, two of which (Campo Imperatore and L'Aquila faults), exhibit high throw-rates exceeding 1 mm/yr (Giraudi and Frezzoti, 1995; Galli et al., 2002; Roberts and Michetti, 2004; Papanikolaou et al., 2005).

4 Active faults surrounding the town of L'Aquila

The town of L'Aquila is not only surrounded by three major active normal faults, but is situated on their hangingwall as well. Each major fault comprises of several overlapping segments, closely spaced parallel segments and even antithetic structures. These antithetic structures all high angle normal faults and closely spaced (∼3–4 km) with the main faults, so that in most cases are linked at depth (Fig. 2). This is the case of the L'Aquila fault that creates a complex fault structure, often leading to different interpretations. The highest damages were recorded in the Aterno valley (Fig. 3a) that is bounded northwards by the L'Aquila fault. The L'Aquila fault is a 37 km long structure that strikes northwest-southeast and downthrows to the southwest (Roberts and Michetti, 2004). Its southern tip is located near Civitaretenga village (2 km east of Caporciano) and its northern tip is located towards the western end of Mt. San Franco (Fig. 2). This fault has a rather complex structure, since it comprises several overlapping segments some of which are antithetic to the main SW dipping fault plane (Papanikolaou et al., 2005). These antithetic planes are nicely observed northwards the village of Barisciano, have fresh looking fault planes and are probably kinematically linked to the NE dipping Bazzano – Fossa fault segments in the southern part of the valley. The Mt. Pettino, the Paganica segment (or Aquilano fault Boncio et al., 2004) and the antithetic Bazzano-Fossa fault outcrop on either side of the valley (Michetti et al., 2000) and form part of the same system.

In a few words the strain in the area is accommodated on multiple closely spaced synthetic and antithetic overlapping segments. Therefore, the fault zone is characterised by distributed displacement on several overlapping faults that break up the footwall and the hanging wall into smaller blocks. This fault has a reported throw-rate of 0.3–0.4 mm/yr (Galadini and Galli, 2000) based on offset Quaternary terraces (Bertini and Bosi, 1993) and up to 1.1 mm/yr towards it centre that decreases to 0.7 mm/yr near Mt. Franco and 0.3 mm/yr towards Caporciano, based on the throws of the postglacial scarps (Papanikolaou et al., 2005). Many Pleistocene palaeolandslides of tectonic origin are reported for this fault concealing the position of the fault trace close to the valley (Demangeot, 1965; Bagnaia et al., 1992).

5 Ground observations and surface ruptures

The earthquake despite its moderate magnitude caused several environmental effects that covered an area of approximately 1000 km^2 (Blumetti et al., 2009; Guzzetti et al., 2009). Most of these effects involved surface ruptures and rockfalls, even though some minor liquefaction and landslide phenomena were also observed. A large number of surface ruptures were recorded in several localities both on

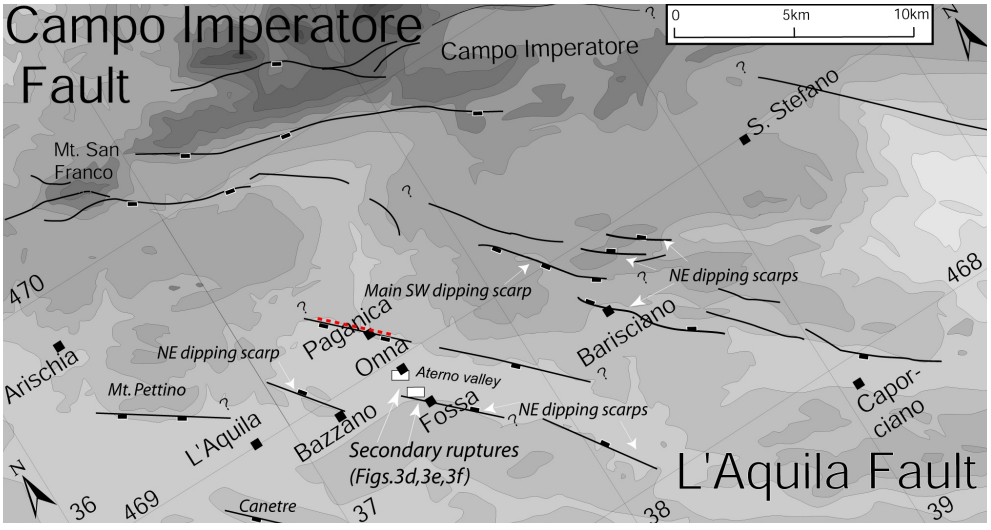

Fig. 2. Detailed topographic map in the L'Aquila area showing the fault segments and the primary surface ruptures with red dashed line (modified from Michetti et al., 2000; Roberts and Michetti, 2004; Papanikolaou et al., 2005).

pre-existing fault planes and within the Aterno Basin (Fig. 3b and c). These ruptures were all NW-SE trending parallel to the activated fault plane as implied also by the focal mechanisms and have throws ranging from a few up to several cm. Several reports describe surface ruptures that occurred on pre-existing fault planes such as the Paganica fault, the Roio – Canetre fault and the NE dipping Bazzano fault, where a 5–8 cm white stripe at the base of the limestone fault scarps were observed (Fig. 3c) and locally on the Mt. Pettino segment and the Campo Imperatore fault (Blumetti et al., 2009; Falcucci et al., 2009, DST Working Group – Uni CHB, 2009; INGV-Emergeo Group, 2009; Michetti et al., 2009). The large amount of ruptures with similar characteristics and displacement values suggest that they can easily confuse which of them are regarded as the primary ruptures. The primary ruptures are the expression of the activated fault plane in the surface, whereas the secondary ruptures are triggered by the earthquake shaking, but are mostly gravitational effects. Secondary ruptures can occur on existing fault planes and/or within basins or within any gravitational or compaction prone formation.

Tens of secondary surface ruptures were widespread within the Aterno basin, reaching up to several tens of meters long (Fig. 3d, e, and f). The Aterno sedimentary basin is characterised by unfavourable site specific conditions. The basin is filled with a few hundred meters of lacustrine sediments that overlie the bedrock (Blumetti et al., 2002), producing significant ground motion amplification effect at low frequencies (De Luca et al., 2005). Most of the secondary ruptures were recorded near the villages of Onna and Fossa. The village of Onna suffered the highest damages (Fig. 3g and h) and recorded the highest death toll (losing 10% of its population), forming the macroseismic intensity epicenter (MCS intensity IX-X, according to Quest, 2009). These secondary ruptures are all strictly NW-SE trending parallel ($150°\pm20°$) to the activated fault plane and the existing fault segments. Following our field campaign immediately after the earthquake, we have been informed by local people that several of the secondary ruptures observed between the villages of Onna and Fossa were created or expanded following the event of the 7 April (M_W=5.6) about 40 h after the mainshock (Fig. 3f). Secondary ruptures were several tens of meters long and up to 30 cm wide and mostly observed near the river as well as on manmade road embankments (Fig. 3d). Overall, these secondary ruptures appeared in artificial and natural structures that are prone to rupturing. Most of these ruptures were transverse to the road network, producing cracks in paved roads that are several meters long and having offsets both horizontal and vertical of several cm (up to 6 cm) (Fig. 3e and f). Their density and length are highly correlated to the damage pattern. This is important because these ruptures are usually disregarded in seismic hazard assessment studies for planning and design purposes.

6 DInSAR analysis

6.1 Methodology

For the purpose of the study ENVISAT ASAR IS2 Single Look Complex (SLC) VV-polarization scenes acquired on 27 April 2008, 1 February 2009, and 12 April 2009 along the descending track 079 were selected. Interferometric processing was performed using GAMMA s/w packages (Wegmüller et al., 1998), forming two coseismic interferometric pairs which span the periods April 2008–April 2009 (080427–090412, 350 days) and February–April 2009

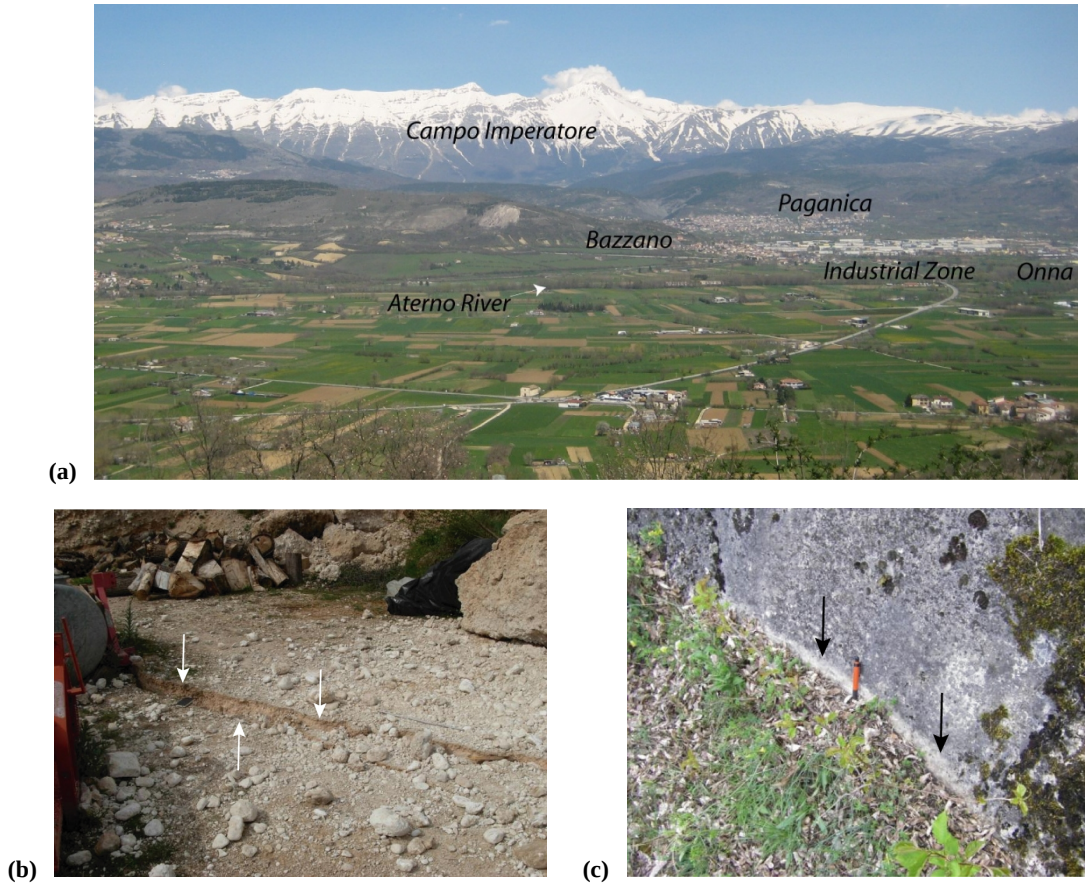

Fig. 3. (a) View of the Aterno Valley and the Campo Imperatore. **(b)** Surface ruptures in Paganica (courtesi E. Vittori), **(c)** surface ruptures in Bazzano (courtesi E. Vittori), **(d)** secondary ruptures within the Aterno valley are several tens of meters long and up to 30 cm wide, near the river embankments, **(e)** transverse ruptures in paved roads that are several meters long and having offsets of several cm (up to 6 cm) both horizontal and vertical. The cracks were violent so that they ruptured also the asphalt pebbles, **(f)** ruptures in a non-paved road between the villages of Onna and Fossa, local people reported to us that these ruptures were formed following the 7 April event (M_W=5.6), **(g)** view of the extended damages and collapses in the village of Onna that was the macroseismic epicentre of the earthquake, **(h)** collapsed bridge about 1 km southeast from the village of Onna.

(090201–090412, 70 days) with a perpendicular baseline of –34.7 m and 157.0 m, respectively. Initial estimates of the interferometric baselines were calculated from available DORIS precise orbit state vectors. State vectors were initially given on 60 s intervals with a default number of 9 state vectors. Due to the insufficient number of state vectors provided, in terms of cover of the area of interest, additional state vectors with an interval of 5.0 s were introduced by respectively interpolation of the available state vectors and orbit propagation. Precision co-registration based on the intensity cross correlation technique was implemented, achieving accuracies of sub-pixel level (∼0.2 pixels). After removal of flat-Earth phases using the estimated interferometric geometry parameter values and refinement of the baselines (Schwäbisch et al., 1995), no phase ramps (orbital fringes) were recognized in the differential interferograms. Topography related phases were simulated based on SRTM V3 DEM of approximate spatial resolution of 90 m, oversampled to 40 m to fit the ASAR data resolution. Athough the area exhibit rugged terrain, small perpendicular baselines ensures the minimization of possible topographic residuals. An adaptive filtering of the differential interferograms based on the local fringe spectrum as proposed by Goldstein and Werner (1998) was considered to assist and reduce possible residues during the unwrapping procedure. Unwrapping of differential phases was performed by applying a Minimum Cost Flow (MCF) algorithm (Costantini, 1998). Finally, accurate geolocation of interferometric results enables not only precise overlays with other data sources in a common map geometry, but also normalisation for the systematic influence of terrain on image radiometry during image co-registration step.

Fig. 3. Continued.

6.2 Results

A number of concentric fringes are clearly visible in both coseismic differential interferograms of the 6 April 2009 earthquake (Fig. 4a and b). The delineation of the surfacial expression of the rupture zone in the area of high fringe rate, reaching the deccorelation threshold, permitted the identification of the activated fault zone. Both patterns/signatures of subsidence up to 25 cm and uplift of about 10 cm along the line of sight (LOS) of the satellite are recognized. The accuracy of the deformation estimates from individual interferograms is mainly limited by the atmospheric path delay term. Visual interpretation of both interferograms, allows the indentification of such artefacts. The basic assumption is that atmosphere, alike other error terms (topography, orbital ramps and signal noise), are uncorrelated between the independent pairs. Atmospheric phases were not identified in any of the generated differential interferograms.

Common acquisition epochs for the coseismic differential interferogram of April 2008–April 2009, in addition to the small values of perpendicular baseline (∼35 m), retain high coherence levels, permitting the interpretation of the differential phases even for a time interval of one year (Fig. 4a). On the contrary and despite the expected high degrees of coherence due to the shorter temporal separation, extend of decorrelation of the April 2008–April 2009 differential interferogram prevents from interpreting the signal especially over the epicentral area. Loss of coherence in the February–April 2009, mainly over the mountainous area in the zone above the tree line where dense vegetation is sparse, is related to the presence of snow in the winter ASAR scene (1 February 2009). The scattering behaviour of the snow changes significantly with snow moisture and with the presence of density heterogeneities. Thus, apart from the visual interpretation for the recognition of atmospheric artefact in the common to the February–April 2009 scene, no further quantitative interpretation was considered for that specific pair (Fig. 4b). Due to the large time span covered by the DInSAR it is possible that pre-seismic deformation can also be superimposed on the co-seismic one. However, the highest pre-seismic event was an M_l=4.1 and is considered to have negligible effects to the DInSAR deformation field compared to the co-seismic event.

The coseismic displacement field revealed by the DInSAR measurements is shown in Fig. 5. The ground deformation pattern is asymmetrical since the deformed area is significantly expanded to the southeast. The observed asymmetry appears in both sides of the activated fault zone. The deformed area is about 460 km^2 with a maximum length of 24 km NW-SE trending along the direction of the rupture plane and a maximum width of 22 km trending NE-SW. This area is shorter in length, but much wider compared to the aftershock distribution. About 66% (or 305 km^2) of the area deformed has been subsided whereas the remaining 34% (or 155 km^2) has been uplifted. The maximum observed uplift

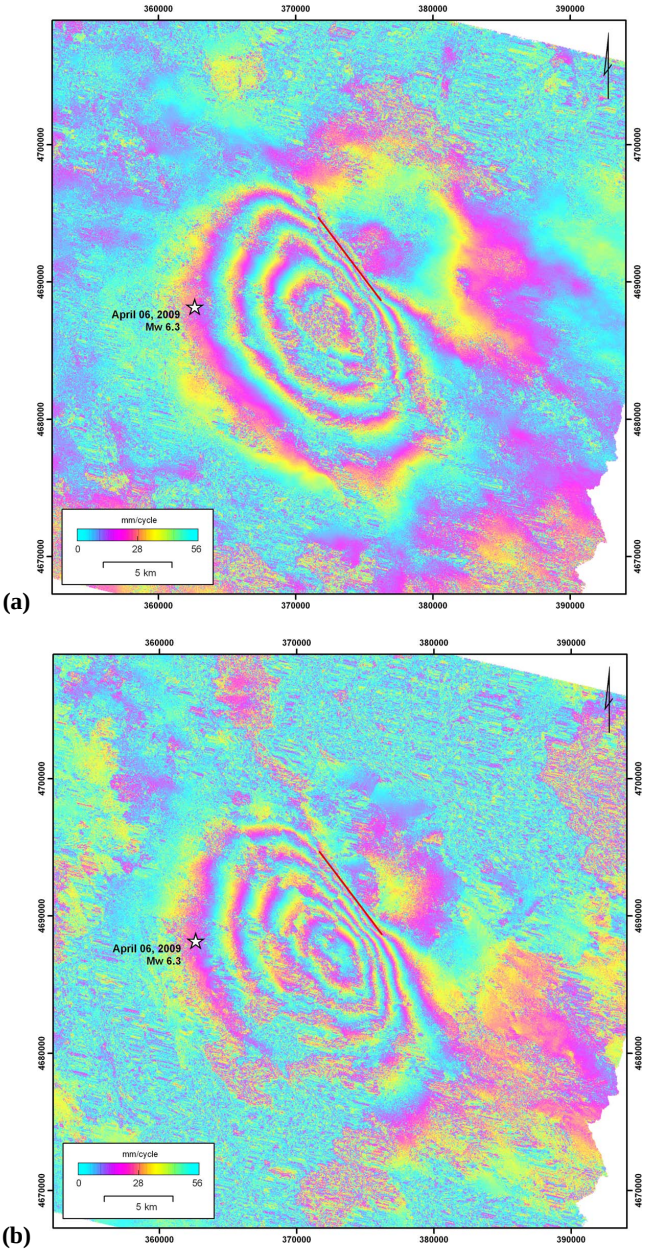

Fig. 4. Coseismic differential interferograms of the April 2009 L'Aquila earthquake, **(a)** covering the periods between April 2008–April 2009 and **(b)** February–April 2009. The trace of the ruptured zone as identified by DInSAR is also shown (red line).

was about 10 cm and was recorded a couple of km northeast from the Paganica surface ruptures in the immediate footwall of the fault, whereas the maximum subsidence was 25 cm and was observed about 2 km SW from the NE dipping Bazzano fault.

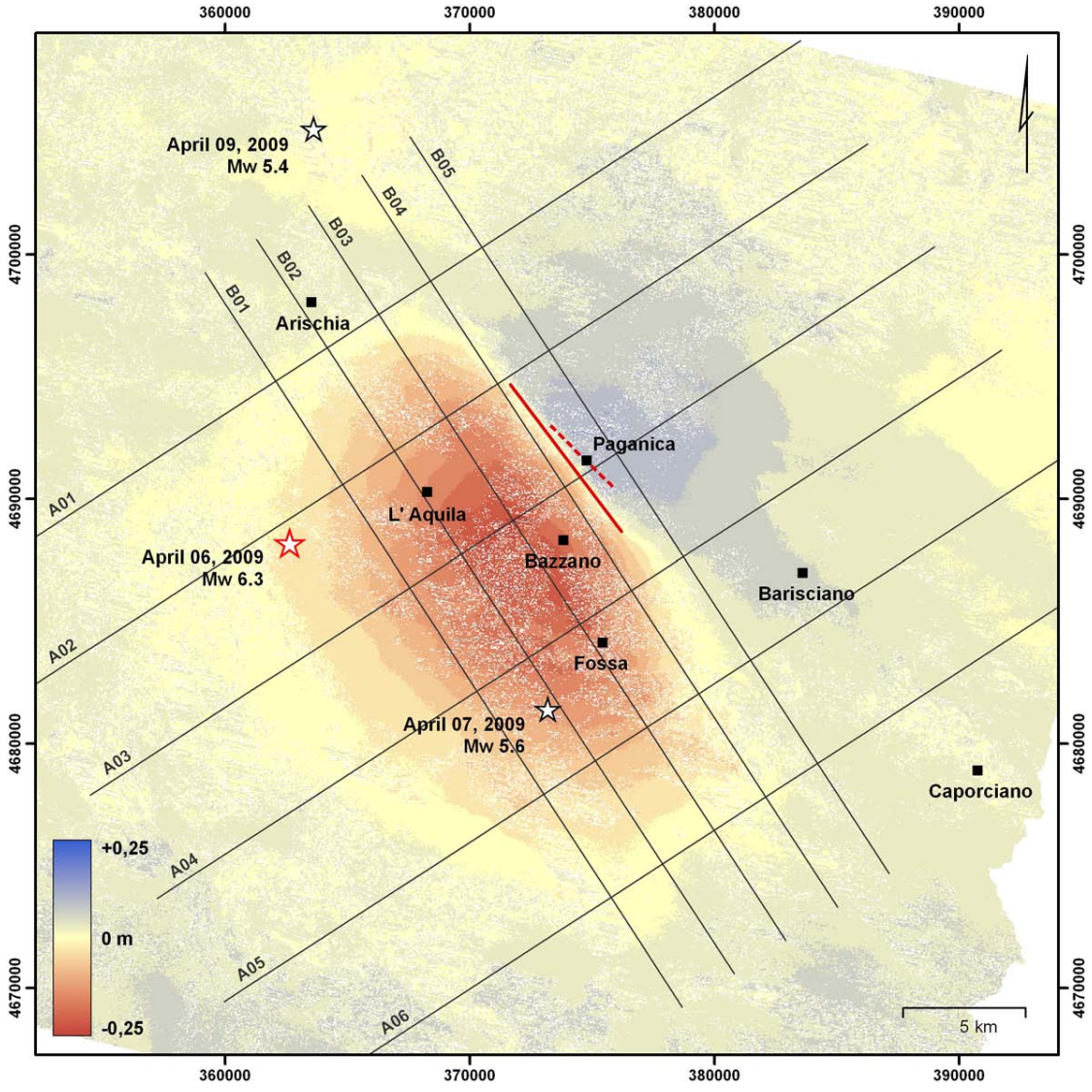

Fig. 5. Displacement field of the 6 and 7 of April 2009 L'Aquila earthquakes. A set of cross sections have been drawn in order to show the differences in deformation both along (profiles B01–B05) and across strike (profiles A01–A06) the activated fault plane. The DInSAR rupture (red line) and the primary surface ruptures (dashed red line) are also projected.

A set of cross sections have been drawn in order to show the differences in deformation both along and across strike the activated fault plane (Figs. 6 and 7). Profiles A01 up to A06 are perpendicular, whereas profiles B01 up to B05 are parallel to the activated fault plane. Profiles A01 up to A06 are 5 km apart from each other, whereas profiles B01 to B05 are 2.5 km apart. Each profile exhibits some interesting features.

Some of the profiles (A01 and A06) are constructed towards the edges of the coseismic displacement field in order to visually interpret the spatial variability of the differential phases for the entire area of interest and especially over the regions of no ground deformation. The stability of the phases in the above areas verifies the reliability of the unwrapping procedure. High frequency oscillations (small wavelength), also visible in the rest of the profiles, correspond to non-earthquake related interferometric disturbances induced mainly by DEM inaccuracies and noise levels in the differential interferograms. Their values, been around ±1.0–1.5 cm, express indirectly the achieved accuracy of the DInSAR measurements.

The profile B05 shows that the pattern is far from symmetrical since the uplift zone is significantly extended towards the SE, even with low values of uplift involved (∼2 cm). Indeed, between 27 and 40 km from the NW towards the second half of the cross section there is a prolonged uplift that correlates with the area influenced by the first large triggered event of the 7 April (M_W=5.6). Therefore, the interferogram

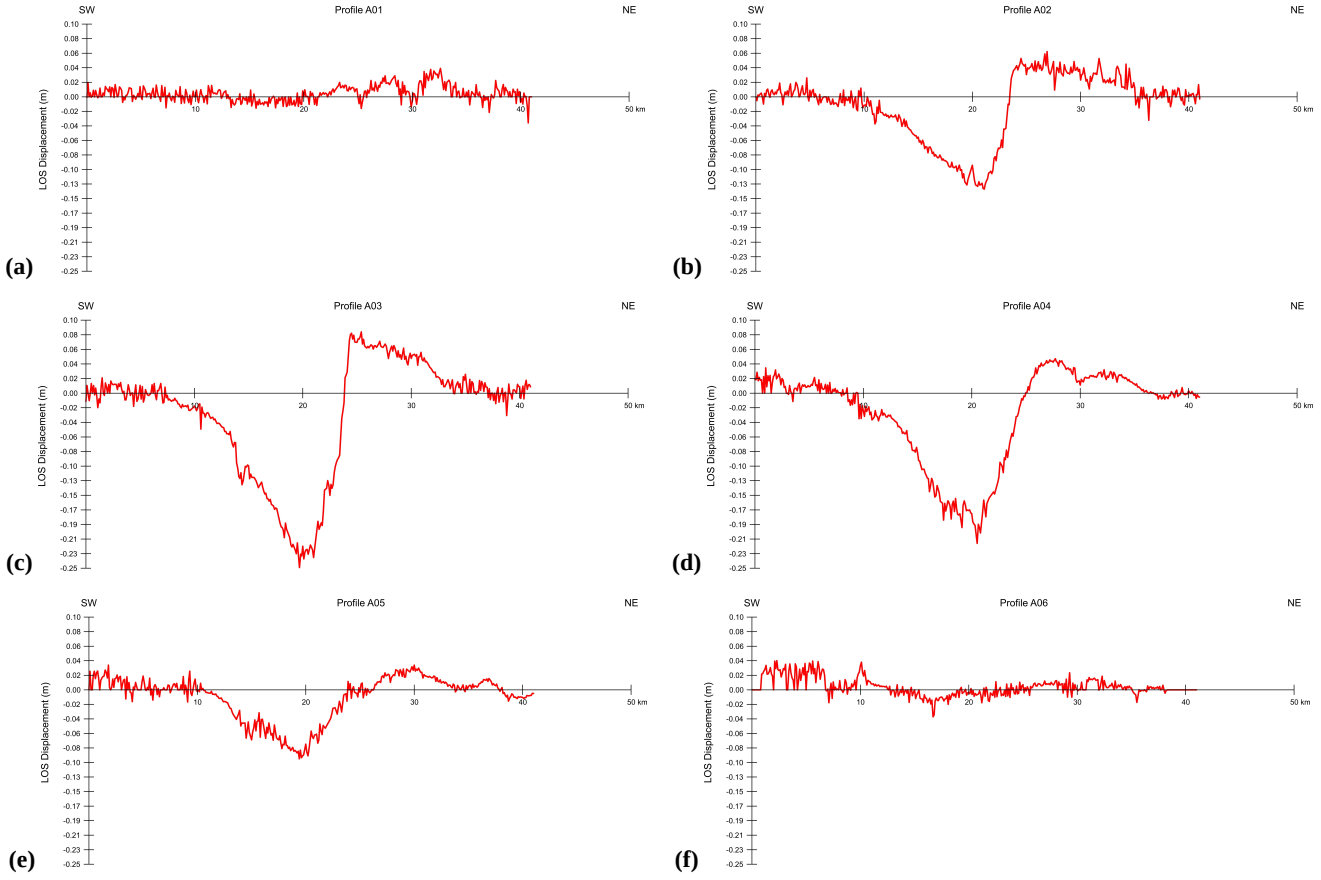

Fig. 6. View of the profiles A01 up to A06 that are perpendicular to the activated fault plane. Profiles are 5 km apart and their traces are shown in Fig. 5. **(a)** Profile A01, **(b)** profile A02, **(c)** profile A03, **(d)** profile A04, **(e)** profile A05, and **(f)** profile A06.

help us infer the influence of this smaller event to the deformation field. The 7 April event activated a zone SW from the mainshock, had a focal depth of approximately 15 km, but a rather unusual seismicity distribution so that its geometry is uncertain (Chiarabba et al., 2009; Pino and Di Luccio, 2009). No fault plane is distinguished by the aftershocks and moreover there is a large gap in the seismicity extending for almost 8 km (e.g. no events between 7 and 15 km depth, source INGV). The same is also true for the other profiles B01 up to B04 towards the hangingwall. Indeed, there is a prolongation of the subsidence also towards the SE. Moreover, the maximum subsidence is observed 9 km away from the epicenter of the mainshock, but only 7 km away from the epicentre of the 7 April event.

Section B04 crosses mostly the immediate hangingwall area, except from its northernmost part where it enters towards the footwall. It is interesting that the maximum subsidence recorded in this section is 15 cm significantly lower to the 24 cm of maximum subsidence recorded in the profile B03, showing that the maximum subsidence is not recorded near the fault trace and the surface ruptures, but closer to the hangingwall centre. It is interesting that even the profiles B01 and B02 which are located further to the southwest in the hanginwall display not only higher subsidence values than the B04 section, but their deformed area is spatially expanded both northwards and southwards. However, part of this subsidence could be attributed to basin effects, soil compaction and overall to gravitational phenomena, even cave collapses so that its distribution may not fully reflect the earthquake characteristics. However, section B05 that shows uplift strengthens our interpretation since uplift can be attributed solely to the earthquake.

Profiles A01 and A06 bound more or less the deformed area. Profile A01 records only about 2–3 cm of uplift, but no subsidence, whereas the profile A06 records a couple of cm both uplift and subsidence. It records also 2–3 cm of uplift towards the southwestern tip of the section. The same effect of uplift but less pronounced, appears also in profiles A04 and A05 towards their southwestern tips, but it dies out in profiles A03 and A02. This uplift feature can not be easily explained, but most probably is related to local unwrapping error. Another possibility could be if the 7 April M_W=5.6 event was not SW dipping as the mainshock, but NE dipping since there are still large uncertainties regarding its geometry

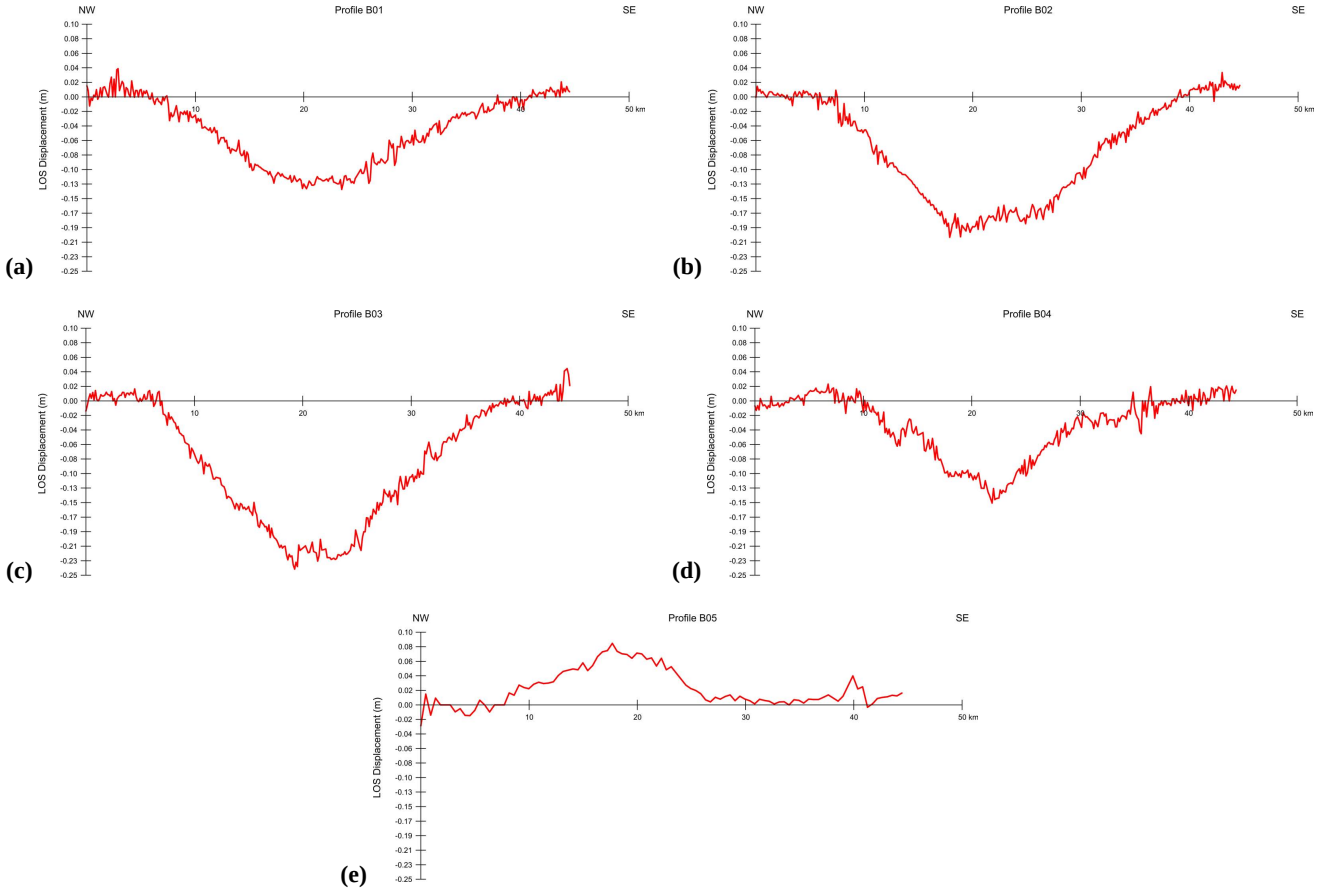

Fig. 7. View of the profiles B01 up to B05 that are parallel to the activated fault plane. Profiles are 2.5 km apart and their traces are shown in Fig. 5. **(a)** Profile B01, **(b)** profile B02, **(c)** profile B03, **(d)** profile B04, and **(e)** profile B05.

(Chiarabba et al., 2009). For example, Pino and Di Luccio (2009) recognize a confused pattern about this event, but they promote a NE dipping solution. This scenario can not be ruled out, however, we think that it is less likely because in such case it is more difficult to explain the substantial and constant uplift observed on the NW part of the A04 and A05 sections as well as the uplift in B05. Moreover, this asymmetry in the DInSAR, which part of it can be attributed to the 7 April event, is expanding spatially both towards the uplift and the subsidence areas. It seems that it is superimposed to the deformation caused by the mainshock deformation, thus favoring a SW dipping solution. Finally, profile A03 crosses through the primary surface ruptures and records the highest uplift and subsidence values.

7 Discussion

The 2009 L'Aquila earthquake (M_W=6.3 or M_L=5.8) in Central Italy, produced both primary and secondary ruptures. Due to the moderate magnitude, primary surface ruptures had small displacements that did not exceed 10 cm. The large amount of ruptures with similar characteristics and displacement values implies that it is difficult to distinguish between primary and secondary ruptures, particularly since several of these ruptures occurred on pre-existing fault planes. This can produce confusion leading to different interpretations on which of the ruptures are primary and which secondary. Such debates occurred in several earthquakes of moderate magnitude in the past such as the 1997 Colfiorito events (M_W=5.7, M_W=6.0) that occurred about 40–50 km north from L'Aquila (Cello et al., 1998; Vittori et al., 2000; Barba and Basili, 2000). The surface ruptures traced in Paganica are considered primary, forming the surface expression of the activated fault. This occurs not only because the Paganica ruptures correlate with well the focal mechanism and the epicenter locality (e.g. Chiarabba et al., 2009), but mainly due to the DInSAR analysis results (see also Atzori et al., 2009; Walters et al., 2009). In particular, the approximately 7 km long DInSAR predicted fault surface ruptures coincide with the surface ruptures observed in Paganica since they are only a couple of hundred meters up to 1 km apart (Fig. 5). Additionally,

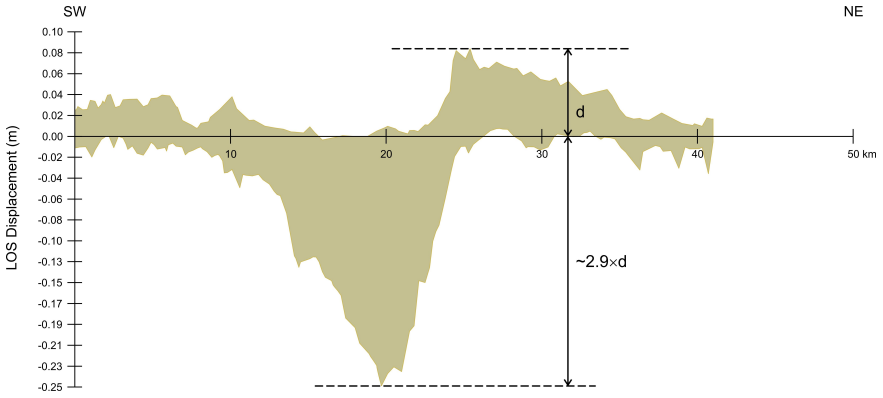

Fig. 8. Diagram showing the range of the observed ground deformation in the epicentral area as appears from all profiles perpendicular to the activated fault plane. A footwall uplift/hangingwall subsidence ratio of about 1/3 with is extracted.

these ruptures broke a 0.7 m diameter high pressure water pipeline in Paganica. Ruptures were discontinuous, but well aligned and could be traced up for at least 2.6 km with maximum displacements not exceeding 10 cm (Michetti et al., 2009; Falcucci et al., 2009, Fig. 3b).

This earthquake has activated one of the fault segments of the L'Aquila fault that bounds the northern part of the Aterno valley in Paganica (Michetti et al., 2000). Boncio et al. (2004) estimated a maximum expected earthquake magnitude of 6.1–6.4 for this segment in Paganica (named it Aquilano fault), which is similar to the mainshock event. Herein, it has to be noted that other fault segments of the same fault system (such as the Mt. Franco, the Barisciano and the Caportiano segments) or other neighboring faults such as the Campo Imperatore and the Barete faults can produce significantly stronger events as implied by their impressive post-glacial fault scarps (Giraudi and Frezzoti, 1995; Papanikolaou et al., 2005). These faults can produce earthquakes $M \geq 6.5$ involving extensive surface ruptures (15–20 km long) with maximum displacements exceeding a meter. Indeed, Galli et al. (2002) based on trenching investigations support that the Campo Imperatore fault that is situated only 20 km away from L'Aquila can give a Magnitude 7.0 earthquake. Finally, the 1703 ($M_W \sim 6.7$) earthquake that damaged L'Aquila (IX intensity), produced surface ruptures >10 km and a maximum displacement of 1 m in the neighbouring Barete fault (Blumetti, 1995). These ruptures are almost one order of magnitude larger than the ruptures produced by the 6 April L'Aquila earthquake, implying that the surrounding faults have the capacity to generate significantly stronger events.

Maximum uplift is about 10 cm whereas the max subsidence is 25 cm. DInSAR values correlate well with GPS recordings from near field GPS stations. The maximum vertical displacement was recorded from a GPS station near the village of Fossa ($\sim$16 cm of subsidence, Anzidei et al., 2009) and is in agreement with the DInSAR values. Figure 8 shows the range of the observed ground deformation in the epicentral area as appears from all profiles. Overall, it is clear that on average there is an uplift/subsidence ratio of about 1/3 with values ranging from 1/2.5 up to 1/3.5. Profiles A02 and A03 that are not influenced by the deformation field of the 7 April earthquake and intersect the ruptured fault, are considered as more reliable regarding the footwall uplift to hangingwall subsidence ratio. Both profiles maintain a 1/3 ratio that involves not only the maximum values, but the entire deformation field along their profiles (Fig. 6b and c). The ratio of footwall uplift to hanging-wall subsidence is relatively poorly known and several different values have been observed and modelled worldwide. For example, Stein and Barrientos (1985) as well as Vita-Finzi and King (1985) suggest that the ratio of footwall uplift to hanging wall subsidence is typically in the range 10–20% (or 1/10–1/5), both for coseismic and longer-term motions. Other scientists have observed uplift to subsidence ratios of 1/2 for the Teton range (Byrd et al., 1994) and the Borah Peak earthquake (Stein et al., 1988). Armijo et al. (1996) used a thick elastic plate model and calculated footwall uplift to hangingwall downdrop ratios of 1/2.7–1/3.5 for the Xylokastro fault in the Corinth Gulf. It is also known that this ratio does not stay constant, but is being modified during the postseismic relaxation (Dalla Via et al., 2003; Kenner and Simons, 2005) where it tends to lower the uplift subsidence differentiation. As a result, it would be very interesting to monitor how this ratio is being modified in time and extract the longer-term ratio. Overall, the value of this ratio is very important particularly for seismic hazard assessment purposes since it governs the fault slip-rates. For example, in some regions such as the Gulf of Corinth and the region of Calabria in Italy the only way to deduce slip-rates covering a long-time period, is from dated uplifted Quaternary marine terraces situated on the footwall of the faults (Bordone and Valensise, 1998; Houghton et al., 2003; Tortrici et al., 2003; Catalano et al., 2003; McNeill and Collier, 2004; De Martini et al., 2004; Ferranti et al., 2007; Roberts et

al., 2009). Due to subsidence the entire hangingwall area is usually located offshore. In such cases, we measure the uplift rate and use the footwall uplift to hangingwall subsidence ratio in order to retrieve the slip-rates.

It is expected that the 7 April M_W=5.6 event has generated its own deformation pattern so that Fig. 5 shows the cumulative deformation field of both events. Atzori et al. (2009) through forward modelling suggest that the large M_W5.6 aftershock has a predicted LOS of 1.5 cm, which is within the assumed data uncertainty. However, similar magnitude shallow (∼10 km depth) normal faulting events (such as the M_W=5.7 1996 Konitsa event in Greece) have produced two full deformation fringes (Nuesch et al., 1999). Therefore, such a magnitude event can produce from 1.5 up to a maximum of 5–6 cm of surface displacement. As a result, the 7 April event may account from 5 up to 17% of the total deformation observed through the DInSAR analysis. Therefore, the deformation produced by the 7 April event has been added up to that of the mainshock, increasing and/or producing this asymmetry in the deformation pattern. The epicentre of the 7 April is much closer to the max subsidence area than the epicentre of the mainshock. Moreover, several of the secondary ruptures observed between the villages of Onna and Fossa were created following the event of the 7 April. Most of the secondary surface ruptures within the Aterno valley were recorded between the villages of Onna and Fossa, where some of the highest subsidence values >18 cm were recorded. Moreover, the area of maximum subsidence does not coincide with the primary surface ruptures that outcrop in Paganica. In particular, the zone of maximum deformation is located about 4.5 km southwest of the primary ruptures. In addition, the fact that the maximum subsidence is located a few km southwards from the NE dipping Bazzano fault that bounds the southwestern part of the recent Aterno valley, suggests that the maximum subsidence is not due to the effect of a possible antithetic structure, but possibly due to the 7 April event. Similar asymmetry of the coseismic displacement field was observed in the case of Athens 1999 $M_s = 5.9$ earthquake (Konotes et al., 2000; Foumelis et al., 2009), attributed to the postseismic deformation, as expressed by the reactivation of the secondary fault zone producing surface deformation of more than a fringe. Overall, aseismic afterslip on the main rupture zone, as well as poroelastic rebound in the shallow crust have a significant contribution on the coseismic displacement field, especially when the examined period covers significant part of the postseismic period/activity (Peltzer et al., 1998, 2001; Peltzer and Crapé, 1999; Donnellan et al., 2002; Liu et al., 2004).

Accelerometer recordings show that the attenuation of PGA with distance is asymmetric with higher decay rate towards the west. The PGA values are stretched to the south east, indicating directivity effects in the rupture propagation (Ameri et al., 2009; Akinci et al., 2009). This strong directivity effect towards the SE revealed by the accelerometers, and the heterogeneous slip distribution (Cirella et al., 2009), favours an inherent asymmetry of the mainshock. One way to find out whether this SE prolongation of the deformation field can be attributed only to the 7 April or not, would be to extract the estimated deformation field of the 7 April event from the cumulative field and trace whether this asymmetry still remains or not. Unfortunately the 7 April event is characterised by high uncertainty regarding its rupture characteristics involving the ruptured area, the fault dip and the estimated slip (e.g. Chiarabba et al., 2009; Pino and Di Luccio, 2009) that such an attempt can not be performed under the present day data. Therefore, a decisive answer can not be provided; however it is very likely that the mainshock is characterized by an inherent asymmetry that became more profound by the generation of the 7 April event.

8 Conclusions

Due to the moderate magnitude, primary surface ruptures had small displacements that did not exceed 10 cm, implying that it was difficult to distinguish between primary and secondary ruptures. The interferogram offers a valuable input in this earthquake, providing a clear view of the surficial deformation pattern since the DInSAR predicted fault surface ruptures coincide with localities where surface ruptures have been observed in the field, confirming that the ruptures observed near Paganica are indeed primary. These ruptures are almost one order of magnitude lower than the ruptures that have been produced by other surrounding faults in the past. Surrounding faults that have not been activated during the 2009 event have the capacity to generate significantly stronger events.

DInSAR analysis shows that 66% (or 305 km^2) of the area deformed has been subsided whereas the remaining 34% (or 155 km^2) has been uplifted. The deformed area (460 km^2) has a maximum length of 24 km NW-SE trending along the direction of the rupture plane and a maximum width of 22 km trending NE-SW, which is shorter in length, but much wider compared to the aftershock distribution. The maximum subsidence (25 cm) was recorded about 4.5 km away from the primary surface ruptures, whereas in the immediate hangingwall (a couple of km from the surface ruptures) subsidence did not exceeded 15 cm, showing that the maximum subsidence is not recorded near the fault trace, but closer to the hangingwall centre.

There is a footwall uplift/hangingwall subsidence ratio of about 1/3. The value of this ratio is important for seismic hazard assessment. It would be very interesting to monitor how this ratio is being modified during the postseismic relaxation period.

An asymmetric deformation pattern has been revealed. The 9 km shift of the observed ground subsidence maxima from the location of the mainshock epicentre and the overall assumetry could be attributed partly to the effect of the first large triggered event M_w=5.6 of 7 April.

Acknowledgements. The authors would like to thank European Space Agency for ENVISAT ASAR scenes provision. This paper benefited from discussions with Gerald Roberts, Dimitrios Papanikolaou, Eutizio Vittori, Luigi Guerrieri, Anna-Maria Blumetti, and Sabina Porfido. Klaire Iossipou is thanked for assistance.

Edited by: M. E. Contadakis
Reviewed by: A. M. Michetti and another anonymous referee

References

Anderson, H. and Jackson, J.: Active tectonics of the Adriatic region, Geophys. J. Roy. Astr. Soc., 91, 937–983, 1987.

Ameri, G., Massa, M., Bindi, D., D'Alema, E., Gorini, A., Luzi, L., Marzorati, S., Pacor, F., Paolucci, R., Puglia, R., and Sferzini, C.: The 6 April 2009 Mw 6.3 L'Aquila (Central Italy) Earthquake: Strong-motion Observations, Seismol. Res. Lett., 80, 951–966, 2009.

Akinci, A., Malagnini, L., and Sabetta, F.: Strong round motion characteristics from the 6 April 2009 L'Aquila earthquake, Italy. Il terremoto Aquilano dell' aprile 2009: primi risultati e strategie future, Chieti, 2009.

Anzidei, M., Boschi, E., Cannelli, V., et al.: Coseismic deformation of the destructive April 6, 2009 L'Aquila earthquake (central Italy) from GPS data, Geophys. Res. Lett., 36, L17307, doi:10.1029/2009GL039145, 2009.

Armijo, R., Meyer, B., King, G., Rigo, A., and Papanastassiou, D.: Quaternary evolution of the Corinth Rift and its implications for the late Cenozoic evolution of the Aegean, Geophys. J. Int., 12, 11–53, 1996.

Atzori, S., Hunstad, I., Chini, M., Salvi, S., Tolomeo, C., Bignami, C., Stramondo, S., Transatti, E., Antonioli, A., and Boschi, E.:. Finite fault inversion of DInSAR coseismic displacement of the 2009 L'Aquila earthquake (central Italy), Geophys. Res. Lett., 36, L15305, doi:10.1029/2009GL039293, 2009.

Bagnaia, R., D'Epifanio, A., and Sylos Labini, S.: Aquila and Subequan basins: an example of Quaternary evolution in Central Apennines, Italy, Quaternaria Nova II, 187–209, 1992.

Barba, S. and Basili, R.: Analysis of seismological and geological observations for moderate-size earthquakes: the Colfiorito Fault System (Central Apennines, Italy), Geophys. J. Int., 141, 241–252, 2000.

Bertini, T. and Bosi, C.: La tettonica quaternaria della conca di Fossa (L'Aquila), Il Quaternario, 6, 293–314, 1993.

Blumetti, A. M.: Neotectonic investigations and evidence of paleoseismicity in the epicentral area of the January–February 1703, Central Italy, earthquakes, in: Perspectives in Paleoseismology, edited by: Serva, L. and Slemmons, D. B., Bulletin of the Association of Engineering Geologists, Special Publication No. 6, 83–100, 1995.

Blumetti, A. M., Di Filippo, M., Zaffiro, P., Marsan, P., and Toro, B.: Seismic hazard of the city of L'Aquila (Abruzzo-Central Italy): new data from geological, morphotectonic and gravity prospecting analysis, Studi Geologici Camerti 1, 7–18, 2002.

Blumetti, A. M., Comerci, V., Di Manna, P., Esposito, E., Guerrieri, L., Piccardi, L., Porfido, S., Vittori, E., Violante, C., Sacchi, M., Berlusconi, A., Livio, F., Michetti, A. M., and Sileo, G.: Gli effetti ambientali della sequenza sismica dell'Aprile 2009 in Abruzzo. Il terremoto Aquilano dell' aprile 2009: primi risultati e strategie future, Chieti, 2009.

Boccaletti, M., Elter, P., and Guazzone, G.: Plate tectonics models for the development of the Western Alps and Northern Apennines, Nature, 234, 108, 1971.

Boncio, P., Lavecchia, G., and Pace, B.: Defining a model of 3D seismogenic sources for seismic hazard assessment applications: The case of central Apennines (Italy), J. Seismol., 8, 407–423, 2004.

Bordoni, P. and Valensise, G.: Deformation of the 125 kyr marine terrace in Italy: tectonic implications, in: Coastal Tectonics, edited by: Stewart, I. S. and Vita-Finzi, C., Geological Society of London Special Publication, 146, 71–110, 1998.

Byrd, O. D., Smith, R. B., and Geissman, J. W.: The Teton fault, Wyoming: Topographic signature, neotectonics, and mechanisms of deformation, J. Geophys. Res., 99, 20095–20122, 1994.

Catalano, S., De Guidi, G., Monaco, C., Tortorici, G., and Tortorici, L.: Long-term behaviour of the Late Quaternari normal faults in the Straits of Messina area (Calabrian arc). Structural and morphological constraints, Quatern. Int., 101–102, 81–91, 2003.

Cavinato, G. P. and De Celles, P. G.: Extensional basins in the tectonically bimodal central Apennines fold-thrust belt, Italy: Response to corner flow above a subducting slab in retrograde motion, Geology, 27, 955–958, 1999.

Cello, G., Deiana, G., Mangano, P., Mazzoli, S., Tondi, E., Ferreli, L., Maschio, L., Michetti, A. M., Serva, L., and Vittory, E.: Evidence for surface faulting during the September 26, 1997, Colfiorito (central Italy) earthquakes, J. Earthq. Eng., 2, 1–22, 1998.

Chiarabba, C., Amato, A., Anselmi, M., et al.: The 2009 L'Aquila (central Italy) M_W 6.3 earthquake: Main shock and aftershocks, Geophys. Res. Lett., 36, L18308, doi:10.1029/2009GL039627, 2009.

Cirella, A., Piatanesi, A., Cocco, M., Tinti, E., Scognamiglio, L., Nichelini, A., Lomax, A., and Boschi, E.: Rupture history of the 2009 L'Aquila (Italy) earthquake from non-linear joint inversion of strong motion and GPS data, Geophys. Res. Lett., 36, L19304, doi:10.1029/2009GL039795, 2009.

Costantini, M: A novel phase unwrapping method based on network programming, IEEE T. Geosci. Remote, 36(3), 813–821, 1998.

De Luca, G., Marcucci, S. Milana, G., and Sano, T.: Evidence of Low-Frequency amplification in the City of L'Aquila, Central Italy, through a multidisciplinary approach includine strong and weak motion data, ambient noise and numerical modeling, B. Seismol. Soc. Am., 95, 1469–1481, 2005.

Dalla Via, G., Sabadini, R., De Natale, G., and Pingue, F.: Lithospheric rheology in southern Italy inferred from postseismic viscoelastic relaxation following the 1980 Irpinia earthquake, J. Geophys. Res., 110, B06311, doi:10.1029/2004JB003539, 2005.

Demangeot, J.: Geomorphologie des Abruzzes Adriatiques, Mémoires et Documents, Centre de Recherches et Documentation Cartographique et Géographique Memoirs et Documents, num. H.s., CNRS Paris, 403 pp., 1965.

De Martini, P. M, Pantosti, D., Palyvos, N., Lemeille, F., McNeill, L., and Collier, R.: Slip rates of the Aigion and Eliki Faults from uplifted marine terraces, Corinth Gulf, Greece Comptes Rendus – Academie des Sciences, Geoscience, 336, 325–334, 2004.

Doglioni, C., Harabaglia, P., Martinelli, G., Mongelli, F., and Zito, G.: A geodynamic model of the Southern Apennines accre-

tionary prism, Terra Nova, 8, 540–547, 1996.

Donnellan, A., Parker, J. W., and Peltzer, G.: Combined GPS and InSAR models of postseismic deformation from the Northridge earthquake, Pure Appl. Geophys., 159, 2261–2270, 2002.

DST Working Group – Uni Ch: Preliminary report: The L'Aquila earthquake of April 2009 (Central Italy) seismotectonic framework and coseismic ground features, Coordinators: Boncio, P., Lavecchia, G., and Pizzi, A., 8 pp., available at: http://www.unich.it/geosis/main/materialeWEB-Aquila/Report.pdf 2009.

Falcucci, E., Gori, S., Peronace, E., Fubelli, G., Moro, M., Saroli, M., Giaccio, B., Messina, P., Naso, G., Scardia, G., Sposato, A., Voltaggio, M., Galli, P., and Galadini, F.: The Paganica Fault and Surface Coseismic Ruptures Caused by the 6 April 2009 Earthquake (L'Aquila, Central Italy), Seismol. Res. Lett., 80, 940–950, 2009.

Ferranti, L., Monaco, C., Antonioli, F., Maschio, L., Kershaw, S., and Verrubbi, V.: The contribution of regional uplift and coseismic slip to the vertical crustal motion in the Messina Straits, southern Italy: Evidence from raised Late Holocene shorelines, J. Geophys. Res., 112, B06401, doi:10.1029/2006JB004473, 2007.

Foumelis, M., Parcharidis, Is., Lagios, E., and Voulgaris, N.: Evolution of post-seismic ground deformation of the Athens 1999 earthquake observed by SAR interferometry, J. Appl. Geophys., 69, 16–23, 2009.

Galadini, F. and Galli, P.: Active tectonics in the Central Apennines (Italy) – Input Data for Seismic Hazard Assessment, Nat. Hazards 22, 225–270, 2000.

Galli, P., Galadini, F., Moro, M., and Giraudi, C.: New paleoseismological data from the Gran Sasso d'Italia area (central Apennines), Geophys. Res. Lett., 29(7), 1134, doi:10.1029/2001GL013292, 2002.

Giraudi, C. and Frezzotti, M.: Paleoseismicity in the Gran Sasso Massif (Abruzzo, Central Italy), Quatern. Int., 25, 81–93, 1995.

GNDT-SSN – Albarello, D., Bosi, V., Bramerini, F., Lucantoni, A., Naso, G., Peruzza, L., Rebez, A., Sabetta, F., and Slejko, D.: New seismic hazard maps of the Italian territory, Gruppo Nazionale per la Difesa dai Terremoti – Servizio Seismico Nazionale, available at: http://www.dstn.it/ssn/PROG/2000/carte_pericolosita/mcs_e.gif, 2001.

Goldstein, R. and Werner, C.: Radar interferogram filtering for geophysical applications, Geophys. Res. Lett., 25(21), 4035–4038, 1998.

Guzzetti, F., Esposito, E., Calducci, V., Porfido, S., Cardinali, M., Violante, C., Fiorucci, F., Sacchi, M., Ardizzone, F., Mondini, A., Reichebach, P., and Rossi, M.: Central Italy seismic sequences induced landsliding: 1997–1998 L'Aquila cases, An international conference in Commemoration of 10th Aniversary of the Chi-Chi Earthquake, 10 pp., 2009.

QUEST(Quick Earthquake Survey Team, Civil Protection Department and INGV): Rapporto sugli effetti del terremoto aquilano del 6 aprile 2009, Rapporto congiunto DPC-INGV, edited by: Galli, P. and Camassi, R., available at: http://www.mi.ingv.it/eq/090406/quest.html, 2009.

INGV(Istituto Nazionale di Geofisica e Vulcanologia): Seismic sequence of the 2009 L'Aquila earthquake, available at: http://www.ingv.it, 2009.

INGV: Database Macrosismico Italiano – DBMIO4, available at: http://emidius.mi.ingv.it/DBMI04/, 2004.

INGV Emergeo working group: Rilievi geologici di terreno effettuati nell'area epicentrale della sequenza sismica dell' Aquilano del 6 aprile 2009, Quaderni di Geophysica, 70, 1–53, 2009.

Houghton, S. L., Roberts, G. P., Papanikolaou, I. D., McArthur, J. M., and Gilmour, M. A.: New 234U-230Th coral dates from the western Gulf of Corinth: implications for extensional tectonics, Geophys. Res. Lett., 30, 2013, doi:10.1029/2003GL018112, 2003.

Kenner, S. J. and Simons, M.: Temporal clustering of major earthquakes along individual faults due to post-seismic reloading, Geophys. J. Int., 160, 179–194, 2005.

Kontoes, C., Briole, P., Sachpazi, M., Veis, G., Elias, P., Sykioti, O., Remy, D., and Kotsis, I.: Displacement field and fault model for the September 7, 1999 Athens earthquake inferred from ERS2 satellite radar Interferometry, Geophys. Res. Lett., 27(24), 3989–3992, 2000.

Liu, G. X., Ding, X. L., Li, Z. L., Li, Z. W., Chen, Y. Q., and Yu, S. B.: Pre- and co-seismic ground deformations of the 1999 Chi-Chi, Taiwan earthquake, measured with SAR interferometry, Comput. Geosci., 30, 333–343, 2004.

Lucente, F. P., C., Chiarabba, G., and Cimini, B.: Tomographic constraints on the geodynamic evolution of the Italian region, J. Geophys. Res., 104, 20307–20327, 1999.

Malinverno, A. and Ryan, W. B. F.: Extension in the Tyrrhenian sea and shortening in the Apennines as result of the arc migration driven by sinking of the lithosphere, Tectonics, 5, 227–245, 1986.

McNeill, L. C. and Collier, R.: Uplift and slip-rates of the eastern Eliki fault segment, Gulf of Corinth, Greece inferred from Holocene and Pleistocene terraces, J. Geol. Soc. London, 161, 81–92, 2004.

Michetti, A. M., Brunamonte, F., Serva, L., and Vittori, E.: Trench investigations of the 1915 Fucino earthquake fault scarps (Abruzzo, Central Italy): geological evidence of large historical events, J. Geophys. Res., 101, 5921–5936, 1996.

Michetti, A. M., Serva, L., and Vittori, E.: ITHACA (Italy hazard from Capable Faulting), a database of active capable faults of the Italian onshore territory, Report of ANPA-Agenzia Nazionale Protezione Ambiente, Rome, 2000.

Michetti, A. M., Vittori, E., Berlusconi, A., Blumetti, A. M., Commerci, V., Di Manna, P., Esposito, E., Guerrieri, L., Livio, F., Porfido, S., and Sileo, G.: Earthquake round effects durino moderate events: The L'Aquila 2009 event case history, 1st INQUA-IGCP-567 International Workshop on Earthquake Archeology and Palaeoseismology, 87–90, 2009.

Nuesch, D., Egli, T., Meier, E., Kahle, H.-G., and Peter, Y.: An application of differential SAR-interferometry (INSAR): The earthquakes from August 1996 in the region of Konitsa (Northern Greece), in: XXII General Assembly of the International Union of Geodesy and Geophysics, IUGG Swiss National Report, available at: http://www.sgc.ethz.ch/iugg99/Section_5.html, 1999.

Pace, B., Peruzza, L., Lavecchia, G., and Boncio, P.: Layered seismogenic source model and probabilistic seismic hazard analyses in central Italy, B. Seismol. Soc. Am., 96, 107–132, 2006.

Papanikolaou, I. D., Roberts, G. P., and Michetti, A. M.: Fault scarps and deformation rates in Lazio-Abruzzo, Central Italy: Comparison between geological fault slip-rate and GPS data, Tectonophysics, 408, 147–176, 2005.

Patacca, E., Sartori, R., and Scandone, P.: Tyrrhenian Basin and

Apenninic Arcs: Kinematic relations since late Tortonian times, Mem. Soc. Geol. It., 45, 425–451, 1990.

Peltzer, G., Rosen, P., and Rogez, F.: Poro-elastic rebound along the Landers 1992 earthquake surface rupture, J. Geophys. Res.-Sol. Ea., 103(B12), 30131–30145, 1998.

Peltzer, G. and Crampé, F.: Evidence of non-linear elasticity of the crust from the Mw7.6 Manyi (Tibet) earthquake surface displacement field, Science, 286(5438), 272–276, 1999.

Peltzer, G., Crampe, F., and Rosen, P.: The Mw 7.1, Hector Mine, California earthquake: surface rupture, surface displacement field, and fault slip solution from ERS SAR data, Comptes Rendus de l'Academie des Sciences A, 333(9), 545–555, 2001.

Pino, N. A. and Di Luccio, F.: Source complexity of the 6 April 2009 L'Aquila (central Italy) earthquake and its strongest aftershock revealed by elementary seismological analysis, Geophys. Res. Lett., 36, L23305, doiQ10.1029/2009GL041331, 2009.

Pondrelli, S., Salimbeni, S., Morelli, A., Ekstrom, G., Olivieri, M., and Boschi, E.: Seismic moment tensors of the April 2009, L'Aquila (central Italy), earthquake sequence, Geophys. J. Int., express letter, 5 pp., doi:10.1111/j.1365-246X.2009.04418.x, 2009.

Oddone, E.: Gli elementi fisica del grande terremoto marsicano fucense del 13 Gennaio 1915, Boll. Soc. Sismol. Ital., 19, 71–215, 1915.

Rebez, A., Sabetta, F., and Slejko, D.: New seismic hazard maps of the Italian territory, Gruppo Nazionale per la Difesa dai Terremoti – Servizio Seismico Nazionale, 2001.

Roberts, G. P., Michetti, A. M., Cowie, P., Morewood, N. C., and Papanikolaou, I.: Fault slip-rate variations during crustal-scale strain localisation, central Italy, Geophys. Res. Lett., 29(8), 9.1–9.4, 10.1029/2001GL013529, 2002.

Roberts, G. P. and Michetti, A. M.: Spatial and temporal variations in growth rates along active normal fault systems: an example from the Lazio-Abruzzo, central Italy, J. Struct. Geol., 26, 339–376, 2004.

Roberts, G. P., Cowie, P., Papanikolaou, I., and Michetti, A. M.: Fault scaling relationships, deformation rates and seismic hazards: An example from the Lazio-Abruzzo Apennines, central Italy, J. Struct. Geol., 26, 377–398, 2004.

Roberts, G. P., Houghton, S. L., Underwood, C., Papanikolaou, I., Cowie, P. A., van Calsteren, T., Wigley, F. J., and Cooper and McArthur, J. M.: Localization of Quaternary slip-rates in an active rift in 10^5 years: An example from central Greece constrained by ^{234}U-^{230}Th coral dates from uplifted paleoshorelines, J. Geophys. Res., 113, B10406, doi:10.1029/2008JB005818, 2009.

Romeo, R. and Pugliese, A.: Seismicity, seismotectonics and seismic hazard of Italy, Eng. Geol., 55, 241–266, 2000.

Schwäbisch, M. and Geudtner, D.: Improvement of phase and coherence map using azimuth prefiltering: Examples from ERS-1 and X-SAR, Proceedings of IGARSS'94, Pasadena, 8–12 August 1995.

Slejko, D., Peruzza, L., and Rebez, A.: Seismic hazard maps of Italy, Ann. Geofis., 41, 183–214, 1998.

Stein, R. S. and Barrientos, S. E.: Planar high-angle faulting in the Basin and Range: geodetic analysis of the 1980 Borah Peak, Idaho, earthquake, J. Geophys. Res., 90, 11355–11366, 1985.

Stein, R. S., King, G. C. P., and Rundle, J. B.: The growth of geological structures by repeated earthquakes. Field examples of continental dip slip faults, J. Geophys. Res., 95, 13319–13331, 1988.

Tertulliani, A., Rossi, A., Cucci, L., and Vecchi, M.: L'Aquila (Central Italy) Earthquakes: The Predecessors of the April 6, 2009 Event, Seismol. Res. Lett., 80, 1008–1013 2009.

Tortorici, G., Bianca, M., De Guidi, G., Monaco, C., and Tortorici, L.: Fault activity and marine terracing in the Capo Vaticano area (southern Calabria) during the middle-late Quaternary, Quatern. Int., 101–102, 269–278, 2003.

Vita-Finzi, C. and King, G. C. P.: The seismicity, geomorphology and structural evolution of the Corinth area of Greece, Philos. T. Roy. Soc. A, 314, 379–407, 1985.

Vittori, E., Deiana, G., Esposito, E., Ferreli, L., Marchegiani, L., Mastrolorenzo, G., Michetti, A. M., Porfido, S., Serva, L., Simonelli, A. L., and Tondi, E.: Ground effects and surface faulting in the September–October 1997 Umbria-Marche (Central Italy) seismic sequence, J. Geodyn., 29, 535–564, 2000.

Walters, R. J., Elliott, J. R., D'Agostino, N., England, P. C., Hunstad, I., Jackson, J. A., Parsons, B., Phillips, R. J., and Roberts, G.: The 2009 L'Aquila earthquake (central Italy): A source mechanism and implications for seismic hazard, Geophys. Res. Lett., 36, L17312, doi:10.1029/2009GL039337, 2009.

Wegmüller, U., Werner, C., and Strozzi, T.: SAR interferometric and SAR differential interferometric processing chain, Proceedings of IGARSS'98, 2, 1106–1108, 1998.